Finite-Difference Analysis of Rectangular Dielectric Waveguide Structures

KARLHEINZ BIERWIRTH, NORBERT SCHULZ, AND FRITZ ARNDT, SENIOR MEMBER, IEEE

Abstract — **A class of dielectric waveguide structures using a rectangular dielectric strip in conjunction with one or more layered dielectrics is analyzed with a finite-difference method formulated directly in terms of the wave equation for the transverse components of the magnetic field. This leads to an eigenvalue problem where the nonphysical, spurious modes do not appear. Moreover, the analysis includes hybrid-mode conversion effects, such as complex waves, at frequencies where the modes are not yet completely bound to the core of the highest dielectric constant, as well as at frequencies below cutoff. Dispersion characteristic examples are calculated for structures suitable for millimeter-wave and optical integrated circuits, such as dielectric image lines, shielded dielectric waveguides, insulated image guides, ridge guides, and inverted strip, channel, strip-slab, and indiffused inverted ridge guides. The numerical examples are verified by results available from other methods.**

I. Introduction

DIELECTRIC WAVEGUIDE structures of the class shown in Fig. 1(a) have found increasing interest for integrated circuit applications in the millimeter-wave and optical frequency range [1]–[21]. As this class includes a wide variety of specially shaped dielectric waveguides (Fig. 1(b)–(k)), in the design of integrated circuits utilizing such structures, it is important to find a reliable computer analysis which is sufficiently general and flexible to allow dominant- and higher order mode solutions of all desired cases and which avoids the troublesome problem of nonphysical or "spurious" modes [28]–[33], [38].

Various methods of analyzing one or several of the structures in Fig. 1(b)–(k) have been the subject of many papers, e.g. [1]–[33], including, in particular, different kinds of mode-matching techniques [2]–[13], [16], [17], [22]–[27] and the finite-element method [15], [28]–[32]. Although the finite-difference method is a common technique for the solution of boundary value problems [33]–[37], it has only been recently [33] that this method has been applied to one of the structures of Fig. 1, the dielectric waveguide (Fig. 1(d)). The variational formulation in [33], however, brings this method close to a finite-element technique [38], and since an $E_z - H_z$ formulation is utilized, spurious modes occur [33].

Following [37], [38] in judging the appropriateness of a method to solve a dielectric waveguide problem with a particular cross-sectional shape, such as that shown in Fig. 1(a) one has to weigh the following criteria: flexibility to deal with a large number of regions and with the hybrid-mode nature of all interesting modes; accuracy and computational efficiency; and the possibility of modifications to eliminate unwanted nonphysical modes. Among the candidates mentioned above, the finite-difference method is considered to meet all these criteria very well.

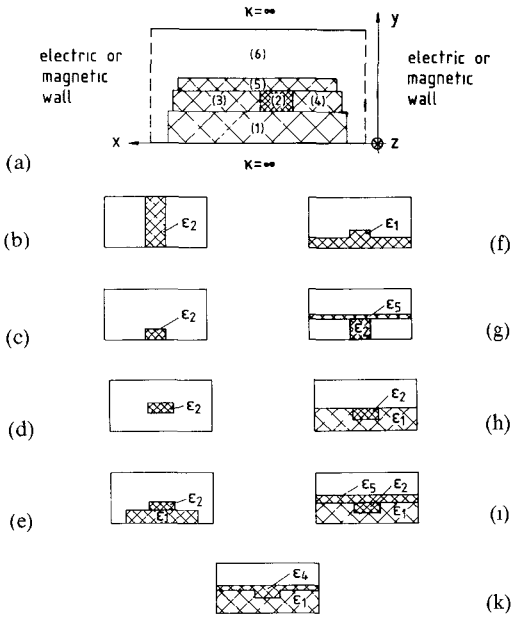

Fig. 1. Layered dielectric waveguide structures for integrated circuits in the millimeter-wave and optical frequency range. (a) General structure. (b) Nonradiative dielectric waveguide (cf. [20]). (c) Dielectric image line ([1]). (d) Dielectric waveguide ([22]). (e) Strip dielectric guide ($\epsilon_2 < \epsilon_1$) or insulated image guide ($\epsilon_2 > \epsilon_1$) ([3]). (f) Ridge guide ([16]). (g) Inverted strip guide ([13]). (h) Channel or embedded strip guide ([2]). (i) Strip-slab guide ([3]). (k) Indiffused inverted ridge guide ([17]).

This paper presents a simple, flexible, versatile finite-difference solution for analyzing the inhomogeneous waveguide structures of Fig. 1 which is free from the problem of spurious modes. Instead of the vector potential formulation of [39], which is solved by searching for the dominant-mode propagation factor [39], a simpler direct wave equation solution formulated in terms of the transverse magnetic field components, H_x and H_y, is utilized which leads advantageously to a conventional eigenvalue problem [40]. A graded mesh permits the investigation of structures with realistic dimensions by making the mesh

Manuscript received March 10, 1986; revised June 24, 1986. This work was supported in part by the Deutsche Forschungsgemeinschaft under Contract No. AR 138/7-1.

The authors are with the Microwave Department of the University of Bremen, Kufsteiner Str., NW-1, D-2800 Bremem 33, West Germany.

IEEE Log Number 8610511.

finer in regions of particular interest; if necessary, the enclosing box is sufficiently large so that it does not perturb the modes perceptibly. Related coupled structures are implicated by suitable electric or magnetic wall symmetry. Moreover, the finite-difference analysis given allows the investigation of hybrid-mode conversion effects, such as complex waves [26], [43]–[45], at frequencies where the modes are not yet completely bound to the core of the highest permittivity, as well as at frequencies below cutoff. Numerical results compared with available data from other methods verify the theory given.

II. Theory

A finite cross section is defined by enclosing the guide in a rectangular box (Fig. 1(a)) where the side walls may be either electric or magnetic walls in order to include coupled structures. An exponential decay factor may be introduced to approximate the infinite exterior region for related "open" structures [28]. Since the finite-difference analysis given includes mode investigations below cutoff, which makes the decay factor modeling difficult to be applied, it is preferred for these cases to make the box large enough [33], [36], [37] so that the influence on the modes may be neglected. A graded mesh permits the optimum use of the available computer capabilities for these cases as well.

The wave equation describing the propagation in a waveguide with inhomogeneous cross section can be expressed in terms of two field components, which are usually taken to be the longitudinal components E_z and H_z [36], [37]. The formulation in terms of the transverse components H_x and H_y is preferred, however, since it circumvents the spurious-mode problem.

The Helmholtz equations in the homogeneous subregions $\nu = 1,2,3,4$ (Fig. 2(a)) are

$$\nabla_t^2 H_x^{(\nu)} + k_\nu^2 H_x^{(\nu)} = 0$$

$$\nabla_t^2 H_y^{(\nu)} + k_\nu^2 H_y^{(\nu)} = 0$$

$$\nabla_t^2 = \frac{\partial^2}{\partial x^2} + \frac{\partial^2}{\partial y_2} \tag{1}$$

where [42]

$$k_\nu^2 = \omega^2 \mu \epsilon_\nu + \gamma^2$$

$$\gamma = \begin{cases} j\beta \\ \alpha \end{cases}$$

and a z dependence of $\exp(-\gamma z)$ of the wave propagation is understood. At the electric or magnetic walls, the boundary conditions $\partial H/\partial n = 0$ or $H = 0$, respectively, have to be satisfied ($\vec{n}$ = unit vector normal to the walls).

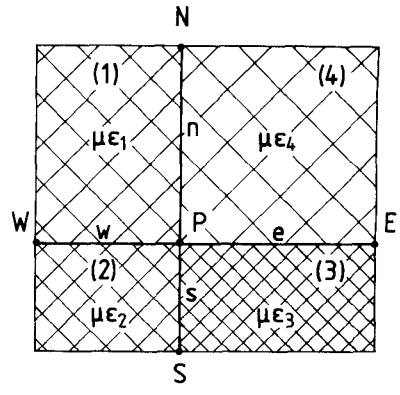

(a)

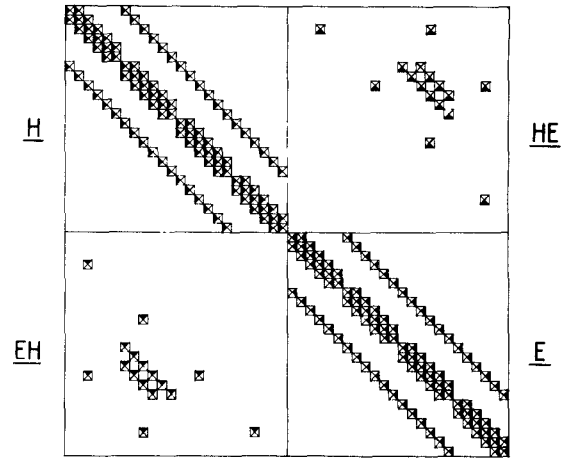

(b)

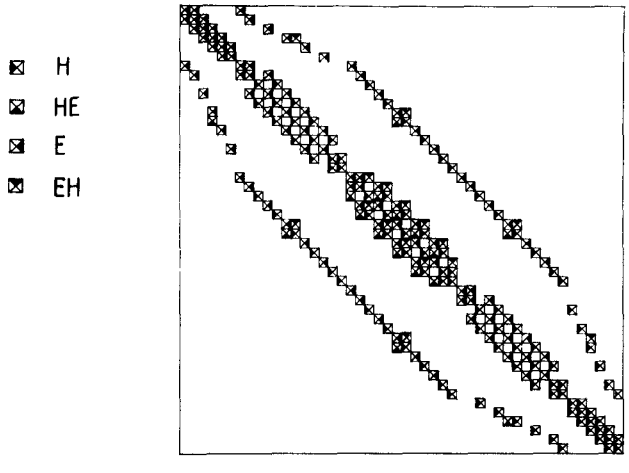

(c)

Fig. 2. Illustration of the finite-difference method treatment. (a) Graded mesh of the five-point representation. (b) Typical original structure of the matrix (A) in (6) and (7). (c) Rearranged structure of (A).

A graded mesh, of side lengths w, n, e, s (Fig. 2(a)), is presumed drawn over the guide cross section. In the general case, there are four subregions with four different dielectric constants. Equations (1) may then be written in its five-point finite-difference form [34], which in the case of inhomogeneous cross sections leads to four coupled

equations for each component H_x or H_y, respectively,

$$0 = -\frac{n}{w}H_W - \frac{w}{n}H_N + \left(\frac{w}{n}+\frac{n}{w}\right)H_P - \frac{1}{2}wnk_1^2H_P + w\frac{\partial H}{\partial y}\bigg|_1 - n\frac{\partial H}{\partial x}\bigg|_1$$

$$0 = -\frac{s}{w}H_W - \frac{w}{s}H_S + \left(\frac{w}{s}+\frac{s}{w}\right)H_P - \frac{1}{2}wsk_2^2H_P - w\frac{\partial H}{\partial y}\bigg|_2 - s\frac{\partial H}{\partial x}\bigg|_2$$

$$0 = -\frac{s}{e}H_E - \frac{e}{s}H_S + \left(\frac{e}{s}+\frac{s}{e}\right)H_P - \frac{1}{2}esk_3^2H_P - e\frac{\partial H}{\partial y}\bigg|_3 + s\frac{\partial H}{\partial x}\bigg|_3$$

$$0 = -\frac{n}{e}H_E - \frac{e}{n}H_N + \left(\frac{n}{e}+\frac{e}{n}\right)H_P - \frac{1}{2}enk_4^2H_P + e\frac{\partial H}{\partial y}\bigg|_4 + n\frac{\partial H}{\partial x}\bigg|_4 \tag{2}$$

where H denotes H_x or H_y, respectively, and the designations W, N, E, S, etc., are elucidated in Fig. 2(a).

Consideration is next given to the boundary conditions for H_x: $E_{z1}=E_{z2}$, $E_{z3}=E_{z4}$, $H_{z1}=H_{z2}$, $H_{z3}=H_{z4}$, $H_{z1}=H_{z4}$, i.e.

$$-\frac{1}{\epsilon_1}\frac{\partial H_x}{\partial y}\bigg|_1 + \frac{1}{\epsilon_2}\frac{\partial H_x}{\partial y}\bigg|_2 + \frac{1}{\epsilon_1}\frac{\partial H_y}{\partial x}\bigg|_1 - \frac{1}{\epsilon_2}\frac{\partial H_y}{\partial x}\bigg|_2 = 0$$

$$\frac{1}{\epsilon_3}\frac{\partial H_x}{\partial y}\bigg|_3 - \frac{1}{\epsilon_4}\frac{\partial H_x}{\partial y}\bigg|_4 - \frac{1}{\epsilon_3}\frac{\partial H_y}{\partial x}\bigg|_3 + \frac{1}{\epsilon_4}\frac{\partial H_y}{\partial x}\bigg|_4 = 0$$

$$\frac{\partial H_x}{\partial x}\bigg|_1 - \frac{\partial H_x}{\partial x}\bigg|_2 + \frac{\partial H_y}{\partial y}\bigg|_1 - \frac{\partial H_y}{\partial y}\bigg|_2 = 0$$

$$\frac{\partial H_x}{\partial x}\bigg|_3 - \frac{\partial H_x}{\partial x}\bigg|_4 + \frac{\partial H_y}{\partial y}\bigg|_3 - \frac{\partial H_y}{\partial y}\bigg|_4 = 0$$

$$\frac{\partial H_x}{\partial x}\bigg|_1 - \frac{\partial H_x}{\partial x}\bigg|_4 + \frac{\partial H_y}{\partial y}\bigg|_1 - \frac{\partial H_y}{\partial y}\bigg|_4 = 0 \tag{3a}$$

and for H_y: $E_{z1}=E_{z4}$, $E_{z2}=E_{z3}$, $H_{z1}=H_{z4}$, $H_{z2}=H_{z3}$, $H_{z1}=H_{z2}$, i.e.

$$-\frac{1}{\epsilon_1}\frac{\partial H_x}{\partial y}\bigg|_1 + \frac{1}{\epsilon_4}\frac{\partial H_x}{\partial y}\bigg|_4 + \frac{1}{\epsilon_1}\frac{\partial H_y}{\partial x}\bigg|_1 - \frac{1}{\epsilon_4}\frac{\partial H_y}{\partial x}\bigg|_4 = 0$$

$$\frac{1}{\epsilon_3}\frac{\partial H_x}{\partial y}\bigg|_3 - \frac{1}{\epsilon_2}\frac{\partial H_x}{\partial y}\bigg|_2 - \frac{1}{\epsilon_3}\frac{\partial H_y}{\partial x}\bigg|_3 + \frac{1}{\epsilon_2}\frac{\partial H_y}{\partial x}\bigg|_2 = 0$$

$$\frac{\partial H_x}{\partial x}\bigg|_1 - \frac{\partial H_x}{\partial x}\bigg|_4 + \frac{\partial H_y}{\partial y}\bigg|_1 - \frac{\partial H_y}{\partial y}\bigg|_4 = 0$$

$$\frac{\partial H_x}{\partial x}\bigg|_3 - \frac{\partial H_x}{\partial x}\bigg|_2 + \frac{\partial H_y}{\partial y}\bigg|_3 - \frac{\partial H_y}{\partial y}\bigg|_2 = 0$$

$$\frac{\partial H_x}{\partial x}\bigg|_2 - \frac{\partial H_x}{\partial x}\bigg|_1 + \frac{\partial H_y}{\partial y}\bigg|_2 - \frac{\partial H_y}{\partial y}\bigg|_1 = 0. \tag{3b}$$

These conditions are satisfactory to properly continue the wave solution from one subregion to the next such that the whole coupled solution governed by Maxwell's equations is obtained. Utilizing these conditions, the finite-difference equations (2) result in

$$\frac{2}{w(w+e)}H_{xW} + \frac{2}{e(w+e)}H_{xE} + \frac{2}{n(w+e)}\left(\frac{w\epsilon_2}{s\epsilon_1+n\epsilon_2}+\frac{e\epsilon_3}{n\epsilon_3+s\epsilon_4}\right)H_{xN} + \frac{2}{s(w+e)}\left(\frac{w\epsilon_1}{s\epsilon_1+n\epsilon_2}+\frac{e\epsilon_4}{n\epsilon_3+s\epsilon_4}\right)H_{xS}$$

$$-\frac{2}{w+e}\left[\frac{\epsilon_1}{s\epsilon_1+n\epsilon_2}\left(\frac{w}{s}+\frac{s}{w}\right)+\frac{\epsilon_2}{s\epsilon_1+n\epsilon_2}\left(\frac{w}{n}+\frac{n}{w}\right)+\frac{\epsilon_3}{n\epsilon_3+s\epsilon_4}\left(\frac{e}{n}+\frac{n}{e}\right)+\frac{\epsilon_4}{n\epsilon_3+s\epsilon_4}\left(\frac{e}{s}+\frac{s}{s}\right)\right]H_{xP}$$

$$+\omega^2\mu\frac{n+s}{w+e}\left(\frac{w\epsilon_1\epsilon_2}{s\epsilon_1+n\epsilon_2}+\frac{e\epsilon_3\epsilon_4}{n\epsilon_3+s\epsilon_4}\right)H_{xP} + \gamma^2H_{xP}$$

$$-\frac{2}{w+e}\frac{\epsilon_1-\epsilon_2}{s\epsilon_1+n\epsilon_2}H_{yW} - \frac{2}{w+e}\frac{\epsilon_3-\epsilon_4}{n\epsilon_3+s\epsilon_4}H_{yE} - \frac{2}{w+e}\left(\frac{\epsilon_2}{s\epsilon_1+n\epsilon_2}-\frac{\epsilon_3}{n\epsilon_3+s\epsilon_4}\right)H_{yN}$$

$$-\frac{2}{w+e}\left(\frac{\epsilon_4}{n\epsilon_3+s\epsilon_4}-\frac{\epsilon_1}{s\epsilon_1+n\epsilon_2}\right)H_{yS} = 0 \tag{4}$$

and

$$\frac{2}{w(n+s)}\left(\frac{s\epsilon_3}{e\epsilon_2+w\epsilon_3}+\frac{n\epsilon_4}{e\epsilon_1+w\epsilon_4}\right)H_{yW}+\frac{2}{e(n+s)}\left(\frac{n\epsilon_1}{e\epsilon_1+w\epsilon_4}+\frac{s\epsilon_2}{e\epsilon_2+w\epsilon_3}\right)H_{yE}+\frac{2}{n(n+s)}H_{yN}+\frac{2}{s(n+s)}H_{yS}$$
$$-\frac{2}{n+s}\left[\frac{\epsilon_1}{e\epsilon_1+w\epsilon_4}\left(\frac{e}{n}+\frac{n}{e}\right)+\frac{\epsilon_2}{e\epsilon_2+w\epsilon_3}\left(\frac{e}{s}+\frac{s}{e}\right)+\frac{\epsilon_3}{e\epsilon_2+w\epsilon_3}\left(\frac{w}{s}+\frac{s}{w}\right)+\frac{\epsilon_4}{e\epsilon_1+w\epsilon_4}\left(\frac{w}{n}+\frac{n}{w}\right)\right]H_{yP}$$
$$+\omega^2\mu\frac{w+e}{n+s}\left(\frac{n\epsilon_1\epsilon_4}{e\epsilon_1+w\epsilon_4}+\frac{s\epsilon_2\epsilon_3}{e\epsilon_2+w\epsilon_3}\right)H_{yP}+\gamma^2H_{yP}$$
$$+\frac{2}{n+s}\left(\frac{\epsilon_3}{e\epsilon_2+w\epsilon_3}-\frac{\epsilon_4}{e\epsilon_1+w\epsilon_4}\right)H_{xW}+\frac{2}{n+s}\left(\frac{\epsilon_1}{e\epsilon_1+w\epsilon_4}-\frac{\epsilon_2}{e\epsilon_2+w\epsilon_3}\right)H_{xE}$$
$$+\frac{2}{n+s}\frac{\epsilon_4-\epsilon_1}{e\epsilon_1+w\epsilon_4}H_{x_N}+\frac{2}{n+s}\frac{\epsilon_2-\epsilon_3}{e\epsilon_2+w\epsilon_3}H_{xS}=0. \tag{5}$$

Equations (4) and (5) give H_{xP} and H_{yP}, the magnetic field components at the discrete node point P, in terms of the immediately adjacent node points W, E, N, S (Fig. 2(a)). These equations are evaluated at each node point P with appropriate modification to include the related boundary conditions (electric or magnetic wall) of the structure to be investigated (Fig. 1(a)). In this way, a set of linear homogeneous equations is derived of the form

$$\begin{pmatrix}(H) & (HE)\\ (EH) & (E)\end{pmatrix}\begin{pmatrix}(H_x)\\ (H_y)\end{pmatrix}=-\gamma^2\begin{pmatrix}(H_x)\\ (H_y)\end{pmatrix} \tag{6}$$

where (H) and (E) denote the submatrices given by the coefficients in (4) and (5) related to H_x or H_y, respectively, whereas (HE) and (EH) denote the coupled terms related to $H_x \leftrightarrow H_y$ and $H_y \leftrightarrow H_x$, respectively. The resulting eigenvalue equation

$$((A)-\lambda(U))(X)=0 \tag{7}$$

where

$$\lambda=-\gamma^2$$
$$(X)=(H_{x1}, H_{x2}, \cdots; H_{y1}, H_{y2}, \cdots)^T$$
$$(A)=\begin{pmatrix}(H) & (HE)\\ (EH) & (E)\end{pmatrix}$$
$$(U)=\text{unity matrix}$$

is solved numerically with routines of the well-known EISPACK package [41]. The original form of (A) (a typical structure is illustrated in Fig. 2(b)) is rearranged in the numerically more convenient form of a banded matrix (Fig. 2(c)). The matrix (A) is real, but not symmetric, and the eigenvalue solutions of (7) may include conjugate complex solutions. For appropriate wave-guiding structures, complex solutions are propagation factors of complex waves, e.g., [26], [43]–[45]. The matrix eigensystem (7) solution by the EISPACK package utilizes the QR-procedure [41], i.e., the decomposition into a product of a unitary matrix Q and the upper right triangular matrix R. The eigenvalues and eigenvectors are found by an iterative process [41], including the complex solutions.

Instead of introducing the boundary conditions given by (3), equivalently satisfactory sets of conditions are possible

$$H_x\colon\ H_{z1}=H_{z4},\ H_{z2}=H_{z3},\ E_{z1}=E_{z4},\ E_{z2}=E_{z3},\ E_{z3}=E_{z4}$$
$$H_y\colon\ H_{z1}=H_{z2},\ H_{z3}=H_{z4},\ E_{z1}=E_{z2},\ E_{z3}=E_{z4},\ E_{z2}=E_{z3}. \tag{8}$$

The third possibility, a mixture of (3) and (8), i.e.

$$H_x\colon\ H_{z1}=H_{z4},\ H_{z2}=H_{z3},\ E_{z1}=E_{z4},\ E_{z2}=E_{z3},\ E_{z3}=E_{z4}$$
$$H_y\colon\ E_{z1}=E_{z4},\ E_{z2}=E_{z3},\ H_{z1}=H_{z4},\ H_{z2}=H_{z3},\ H_{z1}=H_{z2} \tag{9a}$$

or

$$H_x\colon\ E_{z1}=E_{z2},\ E_{z3}=E_{z4},\ H_{z1}=H_{z2},\ H_{z3}=H_{z4},\ H_{z1}=H_{z4}$$
$$H_y\colon\ H_{z1}=H_{z2},\ H_{z3}=H_{z4},\ E_{z1}=E_{z2},\ E_{z3}=E_{z4},\ E_{z2}=E_{z3} \tag{9b}$$

has also been investigated. The boundary conditions given by (8) and (9) lead to expressions similar to those of (4) and (5). The convergence behavior for these three equivalent, but for the numerical treatment somewhat different, cases is illustrated in Fig. 3 in the example of the shielded dielectric image line [26] for the first and the fourth mode. The finite-difference results of the boundary condition sets based on (3) (curve 1), the sets based on (8) (curve 2), and the mixture of the two based on (9a) (curve 3) are plotted against the number N of node points in the x and y direction of a uniform mesh. Equation (9b) leads to nearly identical results with (9a) (curve 3) and therefore is not shown. The results are compared with the mode-matching method [26] for a variable number of higher order modes $M = N/2$ considered in the mode-matching process. Good agreement may be stated for $N = 20$; the relative errors ΔF correspond to the mode-matching solution for $M = 10$. Further, nearly identical convergence behavior for the

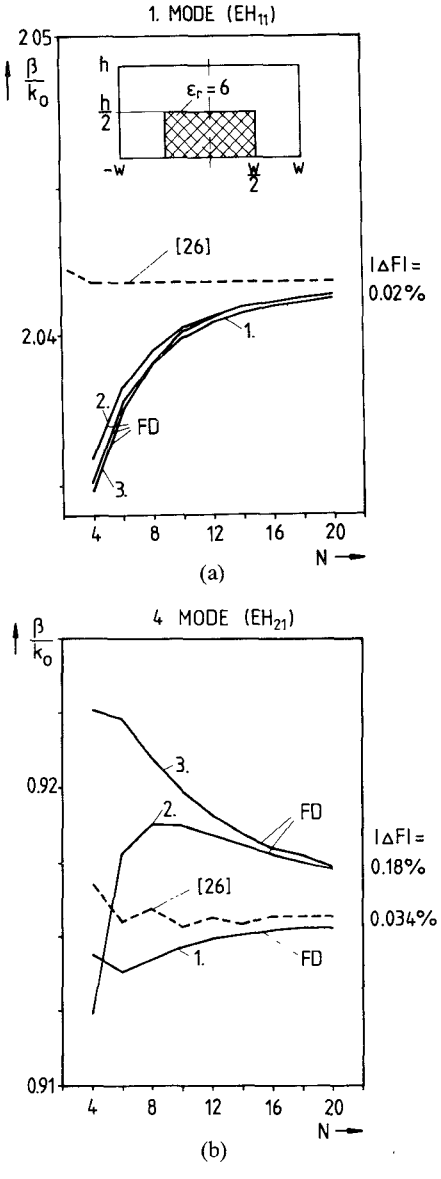

Fig. 3. Convergence behavior of the normalized phase constant β/k_0 (k_0 = free-space wavenumber) versus the number N of node points in x and y direction, respectively. Finite-difference solution for three different sets of boundary conditions (1,2,3), where 1 corresponds to equations (3) and is utilized in this paper. -------- solution of the mode-matching technique of [26] where $M = N/2$ higher order modes are considered. (a) Fundamental mode. (b) Fourth mode.

three boundary sets (curves 1,2,3) may be perceived concerning the fundamental mode (Fig. 3(a)). The same is true for most higher order modes. For some particular modes, however, e.g., the EH_{21} mode, curve 1 (i.e., the boundary conditions of (3)) provides the best convergence; these equations are therefore utilized in this paper.

III. Results

As stated above, the finite-difference formulation in terms of the transverse components H_x and H_y given in (1)–(7) circumvents the spurious-mode problem, in contrast to the formulation in terms of the longitudinal components E_z and H_z. This is demonstrated by Figs. 4 and 5 in the examples of the channel guide (Fig. 4(a) and (b)) and the dielectric waveguide (Fig. 5(a) and (b)). Figs. 4(b) and 5(b), respectively, correspond to the E_z, H_z formulation. Consequently, spurious modes occur, whereas the results of the H_x, H_y formulation (Figs. 4(a) and 5(a)) are free from spurious modes. For the structures under consideration, the mode designations prevailing in the literature have been chosen throughout this paper, i.e., for Figs. 4 and 5 those of [29], [2], and [11].

Good agreement between our results and those of Marcatili [2] may be observed in Fig. 4(a) for the channel guide. This is especially true for higher frequencies, where the approximations of [2] are considered to be more accurate since the field is concentrated increasingly in the regions taken into account in the mode-matching procedure of [2]. To facilitate the comparison, the normalizations B and V_1 [2] for the propagation constant and the frequency, respectively, are used. Concerning the higher order modes, only moderate agreement with [29] is obtained, but like there, an additional H_{41}^y mode may be perceived.

In Fig. 5(a), for the square dielectric waveguide, good agreement between Marcatili's results [2] and our results may be stated, whereas Schweig's results [33], with the exception of the fundamental mode, deviate considerably, especially concerning his "degenerate" modes. The two additionally observed modes between E_{11}^y, E_{21}^y and E_{21}^y,'E_{12}^y are designated with E_{12}^x, E_{21}^x, according to Goell [11]. The comparison with the phase constants of Goell [11] (Fig. 5(c)) shows good agreement. The same is true for a comparison with the available electric wall symmetric results by the mode-matching technique of [23] (Fig. 5(d)). Our calculation of the E_z, H_z formulation for the square dielectric waveguide of high permittivity, Fig. 5(b), indicates that the spurious solutions are found to exist mostly in the range $0.5 < B < 1.0$, as has already been stated in [33] for lower permittivity values. In Fig. 5, the normalized frequency V_2 according to [33] is used. The dispersion curve of the E_{21}^x mode crosses those of the E_{21}^y, E_{12}^x modes (Fig. 5(c)), corresponding to Goell [11]; this effect is increased for higher permittivity values (Fig. 5(a)). The E_{21}^x mode has not been calculated in [2] and [23].

Many examples analyzed by the exact mode-matching technique of [23], [25], and [26] are available for the dielectric image line for many frequency and permittivity ranges. A verification of the finite-difference method by comparison with the previous results for this structure (Fig. 6) is particularly indicated, therefore.

The normalized phase constants β/k_0 (k_0 = free-space wavenumber) versus normalized frequency V_S for a shielded dielectric image line (Fig. 6(a)) agree increasingly well with the related lateral open structure of [23] if the shield dimensions are chosen to be sufficiently large: curve 1 ($d = 2h$, $a = 2w$), curve 2 ($d = 4.8h$, $a = 4.8w$), curve 3 ($d = 4.8h$, $a = 10w$). Deviations are expected near the

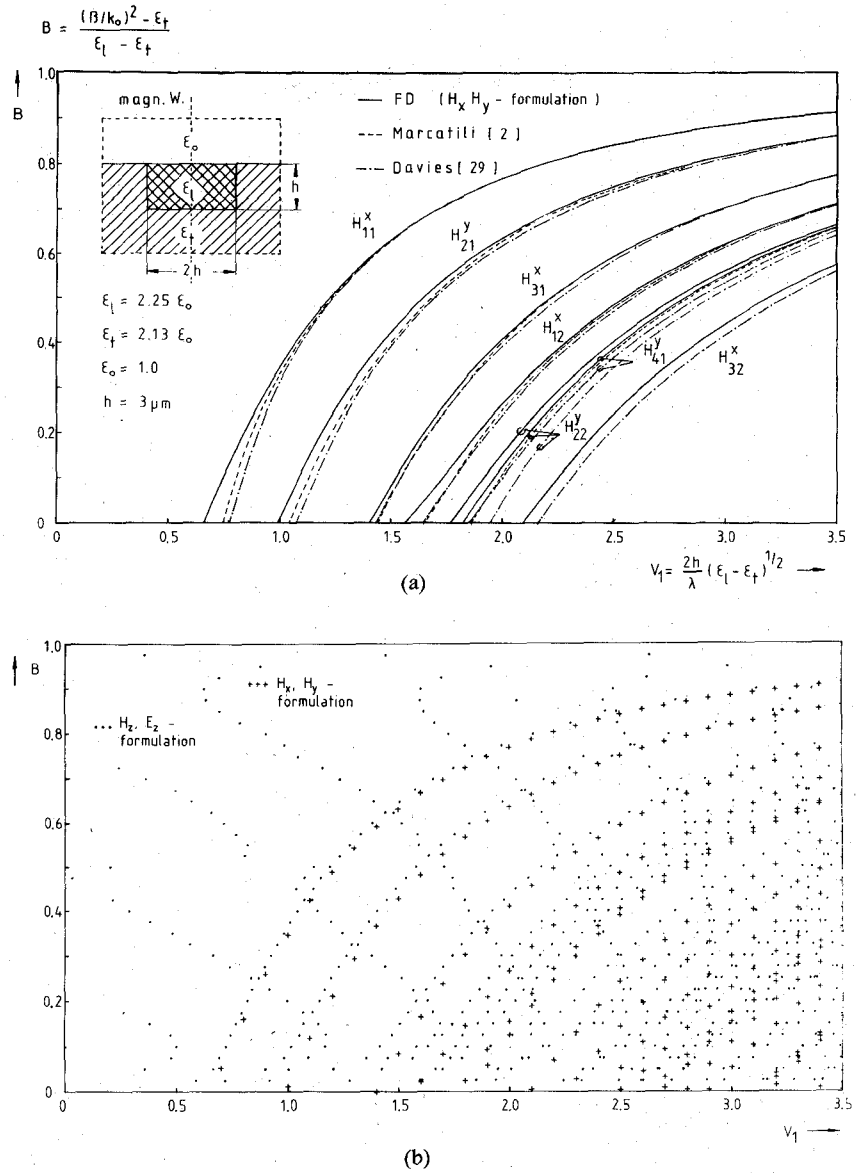

Fig. 4. Channel guide. Normalized propagation constant B versus normalized frequency V_1. (a) Finite-difference formulation in terms of H_x, H_y. (b) Finite-difference formulation in terms of H_z, E_z (own calculations).

cutoff frequency of the fundamental EH_{11} mode because of the influence of the shield, whereas the real open structure [23] exhibits no low-frequency cutoff. The modes are designated according to [23].

Fig. 6(b) shows the propagation constant $\gamma = j\beta$ (or α below cutoff) normalized with k_0 of a dielectric image line shielded with a conventional rectangular *Ku*-band waveguide housing (15.8 mm×7.9 mm). Included is the nonpropagating mode range below the corresponding cutoff frequencies. For simplicity, the corresponding real α values are plotted in the same diagram as in [42], but, for lucidity, in the opposite direction. Between about 13.8 and 16.2 GHz, the eigenvalue solution leads to a complex propagation constant $\gamma_{cw} = \pm \alpha_{cw} \pm j\beta_{cw}$, in spite of the assumption that the shielded image line is lossless. This apparent contradiction is already explained in [26] by complex waves [43], [44], which indicate power transmission with opposite signs: in the forward z direction inside the dielectric region, in the backward direction outside, or vice versa [45]. The affinity to leakage effects stated in [16]–[18] is obvious.

Fig. 6(c), where the normalized propagation constants are plotted against the permittivity ϵ_r, allows the modes to be assigned directly to rectangular waveguide modes ($\epsilon_r = 1$) at finite frequencies (e.g., 14 GHz). A comparison between the finite-difference results and those obtained by the mode-matching method [26] shows good agreement, as indicated in Fig. 6(b) and (c).

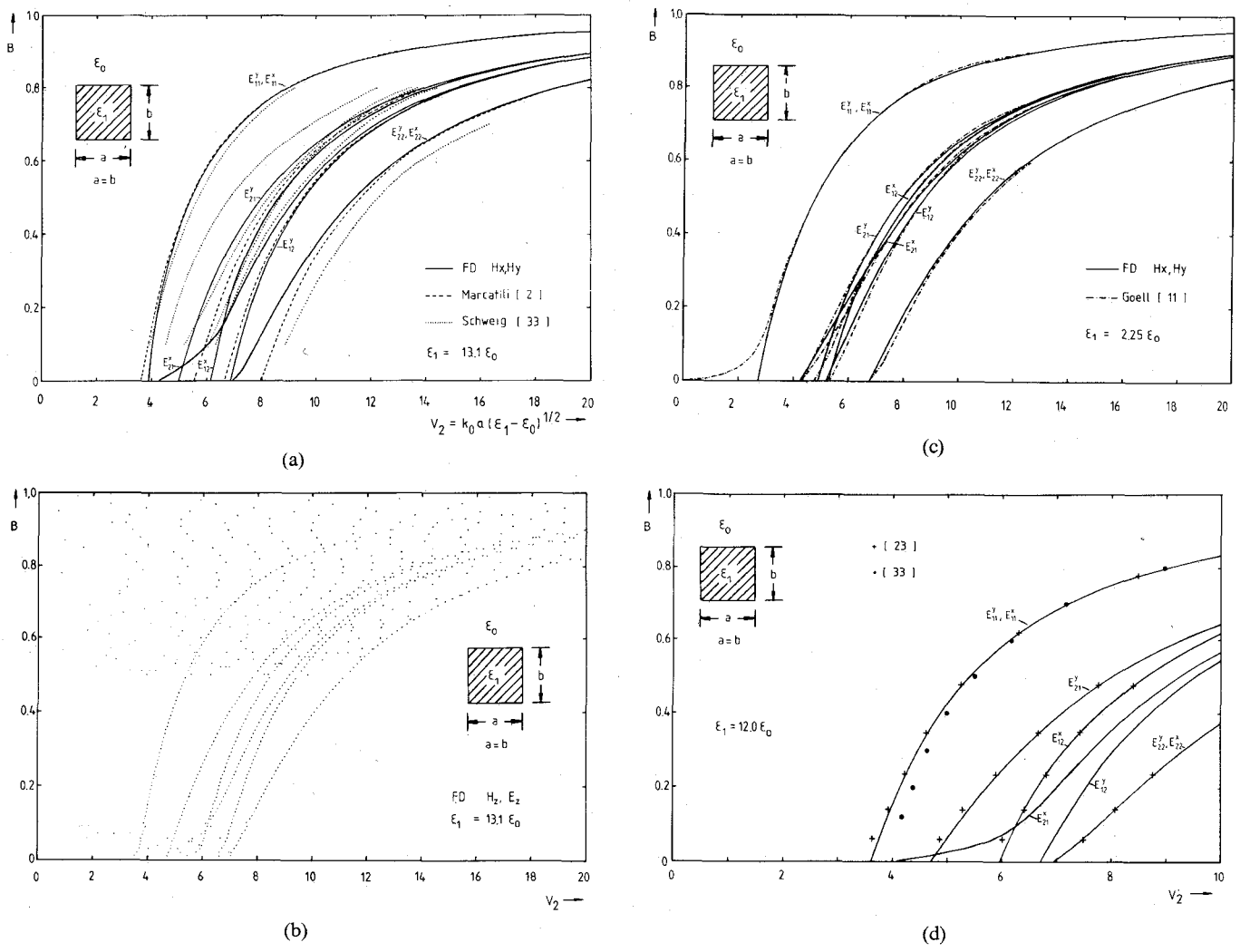

Fig. 5. Dielectric waveguide. Normalized propagation constant B versus normalized frequency V_2, with k_0 the free-space wavenumber. (a) $\epsilon_1 = 13.1\epsilon_0$; comparison with Marcatili [2] and Schweig and Bridges [33]. (b) Finite-difference formulation in terms of H_z, E_z; $\epsilon_1 = 13.1\epsilon_0$ (own calculations). (c) $\epsilon_1 = 2.25\epsilon_0$; comparison with Goell [11]. (d) $\epsilon_1 = 12\epsilon_0$; comparison with Solbach and Wolff [23], and with Schweig and Bridges [33].

Fig. 7 presents normalized propagation constants versus the normalized frequency hk_0 (h = rib height, k_0 = free-space wavenumber) of the ridge guide. The comparison with mode-matching results of [27] shows excellent agreement; this has also been stated for the coupled ridged guide.

For the insulated image guide (Fig. 8), the results of the finite-difference method agree well with the related mode-matching values[1] of [46]. For the inverted strip guide (Fig. 9), excellent agreement with the mode-matching results of [46] is obtained.

Since no spurious modes occur, the finite-difference analysis described here is particularly appropriate for more complicated waveguides, such as the strip-slab guide (Fig. 10).

[1]Note that Fig. 5(a) and (b) in [46] should obviously be interchanged.

IV. Conclusions

A finite-difference analysis for a class of rectangular dielectric waveguide structures is presented which is formulated directly in terms of the simple wave equation for the transverse components of the magnetic fields. This leads to an eigenvalue problem which is free from the troublesome problem of spurious modes. A graded mesh permits the optimum use of the available computer capabilities. The analysis allows the investigation of hybrid-mode conversion effects, such as complex waves, at frequencies where the modes are not yet completely bound to the core of the highest permittivity, as well as at frequen-

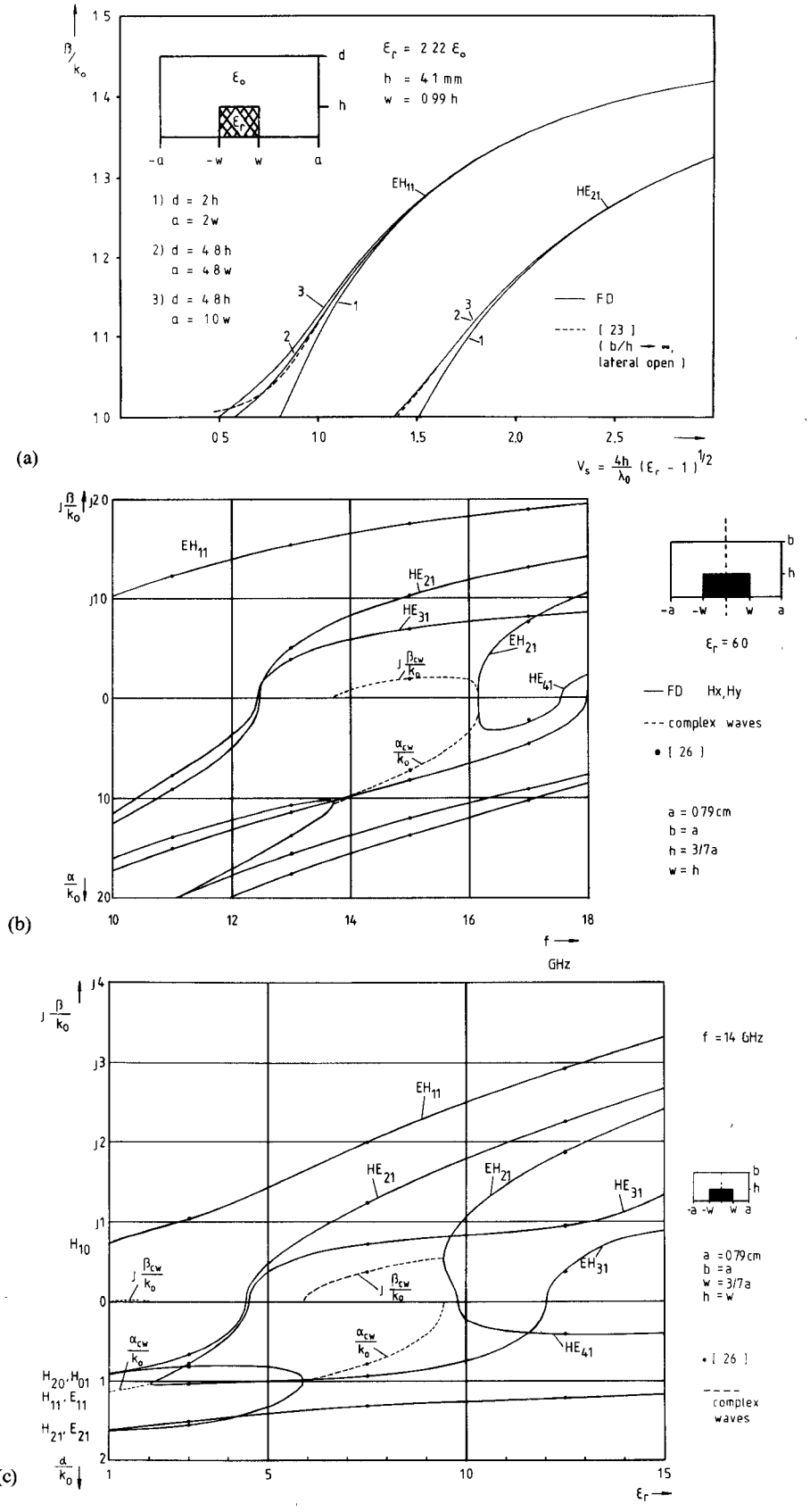

Fig. 6. Dielectric image line. (a) Normalized phase constant β/k_0 (k_0 = free-space wavenumber) versus normalized frequency. Approximation of the lateral open structure of [23] by shield dimensions 1) $d = 2h$, $a = 2w$; 2) $d = 4.8h$, $a = 4.8w$; 3) $d = 4.8h$, $a = 10w$. (b) Propagation constant $\gamma = \{j\beta; \alpha\}$ normalized to k_0 plotted against frequency; $\epsilon_r = 6$; shield dimensions $2a = 15.799$ mm, $b = a$ (*Ku*-band waveguide housing). -------- complex wave. (c) Propagation constant $\gamma = \{j\beta; \alpha\}$ normalized to k_0 plotted against permittivity ϵ_r; $f = 14$ GHz. ---------- complex waves.

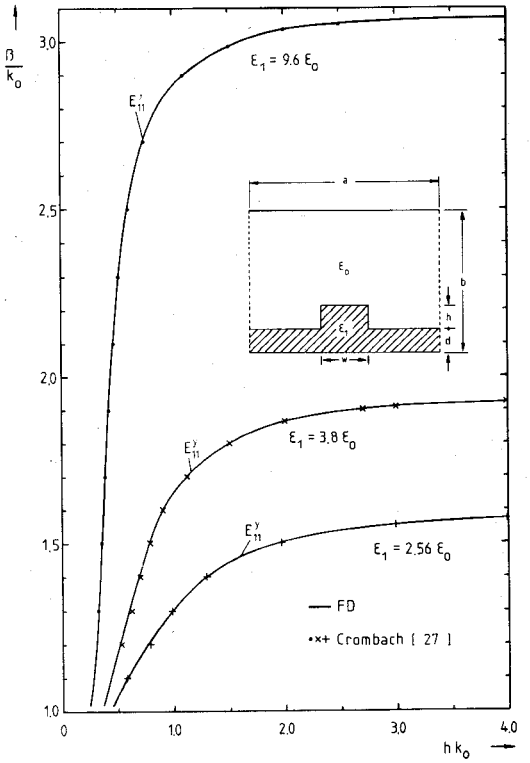

Fig. 7. Ridge guide with $w = 2h$, $d = h$, $a = 100h$, and $b = 6h$. Normalized propagation constant versus normalized frequency (h = rib height, k_0 = free-space wavenumber) for different permittivities.

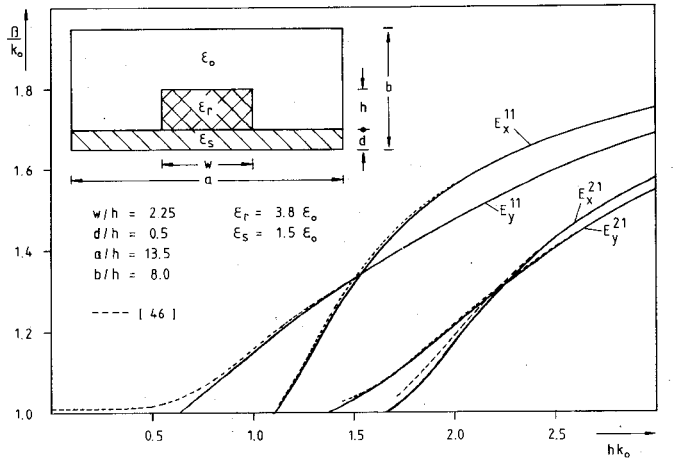

Fig. 8. Insulated image guide with structure according to [46]. Normalized propagation constant versus normalized frequency.

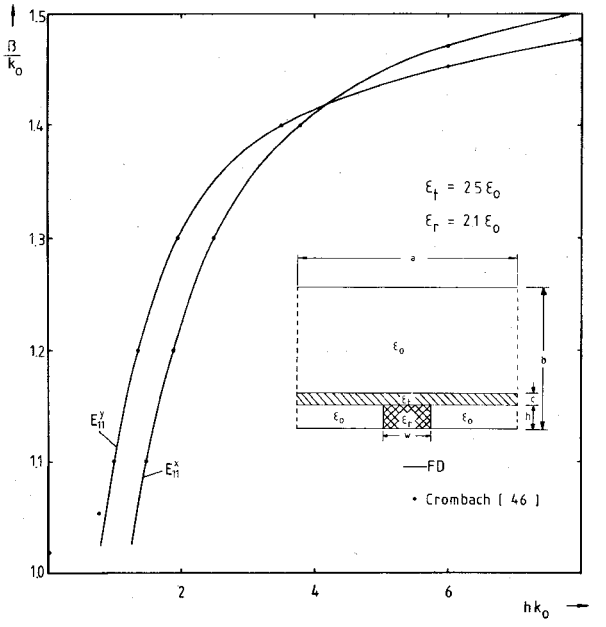

Fig. 9. Inverted strip guide. Normalized propagation constant versus normalized frequency (h = inverted strip height, k_0 = free-space wavenumber): $w/h = 2$, $c/h = 0.5$, $b/h = 8$, $a/b = 20$.

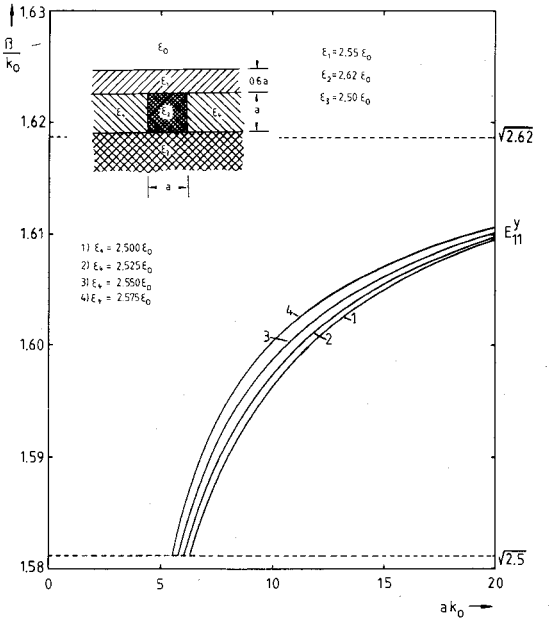

Fig. 10. Strip-slab guide. Normalized propagation constant versus normalized frequency (a = strip height, k_0 = free-space wavenumber); single structure with different permittivity values for ϵ_4.

cies below cutoff. The calculated dispersion curves compare well with results available from other methods.

References

[1] D. D. King, "Circuit components in dielectric images lines," *IRE Trans. Microwave Theory Tech.*, vol. MTT-3, pp. 35–39, Dec. 1955.

[2] E. A. J. Marcatili, "Dielectric rectangular waveguide and directional coupler for integrated optics," *Bell Syst. Tech. J.*, vol. 48, pp. 2071–2102, Sept. 1969.

[3] W. V. McLevidge, T. Itoh, and R. Mittra, "New waveguide structures for millimeter-wave and optical integrated circuits," *IEEE Trans. Microwave Theory Tech.*, vol. MTT-23, pp. 788–794, Oct. 1975.

[4] R. M. Knox, "Dielectric waveguide microwave integrated circuits —An overview," *IEEE Trans. Microwave Theory Tech.*, vol. MTT-24, pp. 806–814, Nov. 1976.

[5] T. Itoh, "Application of gratings in a dielectric waveguide for leaky-wave antennas and band-reject filters," *IEEE Trans. Microwave Theory Tech.*, vol. MTT-25, pp. 1134–1138, Dec. 1977.

[6] J. A. Paul and Y.-W. Chang, "Millimeter wave image-guide integrated passive devices," *IEEE Trans. Microwave Theory Tech.*, vol. MTT-26, pp. 751–754, Oct. 1978.

[7] K. Solbach, "The calculation and the measurements of the coupling properties of dielectric image lines of rectangular cross section," *IEEE Trans. Microwave Theory Tech.*, vol. MTT-27, pp. 54–58, Jan. 1979.

[8] J. A. Paul and P. C. H. Yen, "Millimeter-wave components and

six-port network analyzer in dielectric waveguide," *IEEE Trans. Microwave Theory Tech.*, vol. MTT-29, pp. 948–954, Sept. 1981.
[9] T. Itoh, "Open guiding structures for mmW integrated circuits," *Microwave J.*, pp. 113–126, Sept. 1982.
[10] S. E. Miller, "Integrated optics: An introduction," *Bell Syst. Tech. J.*, vol. 48, pp. 2059–2069, Sept. 1969.
[11] J. E. Goell, "A circular-harmonic computer analysis of rectangular dielectric waveguides," *Bell Syst. Tech. J.*, vol. 48, pp. 2133–2160, Sept. 1969.
[12] R. M. Knox and P. D. Toulios, "Integrated circuits for the millimeter through optical frequency range," in *Proc. of the Symp. Submillimeter Waves* (New York), Mar. 1970, pp. 497–516.
[13] T. Itoh, "Inverted strip dielectric waveguide for millimeter-wave integrated circuits," *IEEE Trans. Microwave Theory Tech.*, vol. MTT-24, pp. 821–827, Nov. 1976.
[14] R. M. Knox, "Dielectric waveguides: A low-cost option for IC's," *Microwaves*, pp. 56–64, Mar. 1976.
[15] M. Ikeuchi, H. Swami, and H. Niki, "Analysis of open-type dielectric waveguides by the finite element iterative method," *IEEE Trans. Microwave Theory Tech.*, vol. MTT-29, pp. 234–239, Mar. 1981.
[16] S.-T. Peng and A. A. Oliner, "Guidance and leakage properties of a class of open dielectric waveguides: Part I—Mathematical formulations," *IEEE Trans. Microwave Theory Tech.*, vol. MTT-29, pp. 843–855, Sept. 1981.
[17] A. A. Oliner, S.-T. Peng, T. I. Hsu, and A. Sanchez, "Guidance and leakage properties of a class of open dielectric waveguides: Part II —New physical effects," *IEEE Trans. Microwave Theory Tech.*, vol. MTT-29, pp. 855–869, Sept. 1981.
[18] G. L. Matthaei, "A note concerning modes in dielectric waveguide gratings for filter applications," *IEEE Trans. Microwave Theory Tech.*, vol. MTT-31, pp. 309–312, Mar. 1983.
[19] G. L. Matthaei, D. Park, Y. M. Kim, and D. L. Johnson, "A study of the filter properties of single and parallel-coupled dielectric-waveguide gratings," *IEEE Trans. Microwave Theory Tech.*, vol. MTT-31, pp. 825–835, Oct. 1983.
[20] T. Yoneya and S. Nishida, "Nonradiative dielectric waveguide for millimeter-wave integrated circuits," *IEEE Trans. Microwave Theory Tech.*, vol. MTT-29, pp. 1188–1192, Nov. 1981.
[21] T. Yoneyama, F. Kuroki, and S. Nishida, "Design of nonradiative dielectric waveguide filters," *IEEE Trans. Microwave Theory Tech.*, vol. MTT-32, pp. 1659–1662, Dec. 1984.
[22] W. O. Schlosser and H. G. Unger, "Partially filled waveguides and surface waveguides of rectangular cross section," in *Advances in Microwaves*, vol. 1. New York: Academic Press, 1966, pp. 319–387.
[23] K. Solbach and I. Wolff, "The electromagnetic fields and the phase constants of dielectric image lines," *IEEE Trans. Microwave Theory Tech.*, vol. MTT-26, pp. 266–274, Apr. 1978.
[24] N. Deo and R. Mittra, "A technique for analyzing planar dielectric waveguides for millimeter wave integrated circuits," *Arch. Elek. Übertragung*, vol. 37, pp. 236–244, July/Aug. 1983.
[25] J. Strube and F. Arndt, "Three-dimensional higher-order mode analysis of transition from waveguide to shielded dielectric image line," *Electron. Lett.*, vol. 19, pp. 306–307, Apr. 1983.
[26] J. Strube and F. Arndt, "Rigorous hybrid-mode analysis of the transition from rectangular waveguide to shielded dielectric image guide," *IEEE Trans. Microwave Theory Tech.*, vol. MTT-33, pp. 391–401, May 1985.
[27] U. Crombach, "Analysis of single and coupled rectangular dielectric waveguides," *IEEE Trans. Microwave Theory Tech.*, vol. MTT-29, pp. 870–874, Sept. 1981.
[28] B. M. A. Rahman and J. B. Davies, "Finite-element analysis of optical and microwave waveguide problems," *IEEE Trans. Microwave Theory Tech.*, vol. MTT-32, pp. 20–28, Jan. 1984.
[29] B. M. A. Rahman and J. B. Davies, "Penalty function improvement of waveguide solution by finite elements," *IEEE Trans. Microwave Theory Tech.*, vol. MTT-32, pp. 922–928, Aug. 1984.
[30] B. M. A. Rahman and J. B. Davies, "Finite-element solution of integrated optical waveguides," *J. Lightwave Technol.*, vol. LT-2, pp. 682–687, Oct. 1984.
[31] M. Koshiba, K. Hayata, and M. Suzuki, "Approximate scalar finite-element analysis of anisotropic optical waveguides with off-diagonal elements in a permittivity tensor," *IEEE Trans. Microwave Theory Tech.*, vol. MTT-32, pp. 587–593, June 1984.
[32] M. Koshiba, K. Hayata, and M. Suzuki, "Improved finite-element formulation in terms of the magnetic field vector for dielectric waveguides," *IEEE Trans. Microwave Theory Tech.*, vol. MTT-33, pp. 227–233, Mar. 1985.
[33] E. Schweig and W. B. Bridges, "Computer analysis of dielectric waveguides: A finite-difference method," *IEEE Trans. Microwave Theory Tech.*, vol. MTT-32, pp. 531–541, May 1984.
[34] J. B. Davies and C. A. Muilwyk, "Numerical solution of uniform hollow waveguides of arbitrary shape," *Proc. Inst. Elec. Eng.*, vol. 113, pp. 277–284, Feb. 1966.
[35] M. J. Baubien and A. Wexler, "An accurate finite-difference method for higher order waveguide modes," *IEEE Trans. Microwave Theory Tech.*, vol. MTT-16, pp. 1007–1017, Dec. 1968.
[36] J. S. Hornsby and A. Gopinath, "Numerical analysis of a dielectric-loaded waveguide with a microstrip line—Finite difference methods," *IEEE Trans. Microwave Theory Tech.*, vol. MTT-17, pp. 684–690, Sept. 1969.
[37] D. G. Corr and J. B. Davies, "Computer analysis of the fundamental and higher order modes in single and coupled microstrip," *IEEE Trans. Microwave Theory Tech.*, vol. MTT-20, pp. 669–678, Oct. 1972.
[38] S. M. Saad, "Review of numerical methods for the analysis of arbitrarily-shaped microwave and optical dielectric waveguides," *IEEE Trans. Microwave Theory Tech.*, vol. MTT-33, pp. 894–899, Oct. 1985.
[39] J.-D. Decotignie, O. Parriaux, and F. Gardiol, "Birefringence properties of twin-core fibers by finite differences," *J. Opt. Commun.*, vol. 3, no. 1, pp. 8–12, Mar. 1982.
[40] C. G. Williams and G. K. Cambrell, "Numerical solution of surface waveguide modes using transverse field components," *IEEE Trans. Microwave Theory Tech.*, vol. MTT-22, pp. 329–330, Mar. 1974.
[41] B. S. Garbow, J. M. Boyle, J. J. Dougarra, and C. B. Moler, "Matrix eigensystem routines—EISPACK guide extension," in *Lecture Notes in Computer Science*, vol. 51. Heidelberg: Springer-Verlag, 1977.
[42] R. F. Harrington, *Time-Harmonic Electromagnetic Fields*. New York: McGraw-Hill, 1961, ch. 2.7.
[43] P. J. B. Clarricoats and K. R. Slinn, "Complex modes of propagation in dielectric loaded circular waveguide," *Electron. Lett.*, vol. 1, pp. 145–146, 1965.
[44] V. A. Kalmyk, S. B. Rayevskiy, and V. P. Ygvyumov, "An experimental verification of existence of complex waves in a two-layer circular, shielded waveguide," *Radio Eng. Electron. Phys.*, vol. 23, pp. 16–19, 1978.
[45] H. Katzier and F. J. K. Lange, "Grundlegende Eigenschaften komplexer Wellen am Beispiel der geschirmten kreiszylindrischen dielektrischen Leitung," *Arch. Elek. Übertragung*, vol. 37, pp. 1–5, Jan./Feb. 1983.
[46] U. Crombach, "Wellentypen auf einzelnen und gekoppelten dielektrischen Wellenleitern," *Frequenz*, vol. 39, pp. 26–33, Jan./Feb. 1985.

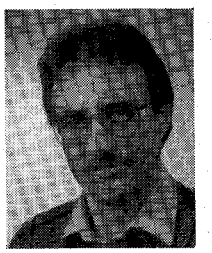

Karlheinz Bierwirth was born in Leverkusen, Germany, on April 5, 1957. He received the Dipl. Ing. degree from the University of Bremen, Germany, in 1983.

Since 1983, he has been with the Microwave Department of the University of Bremen, where he is engaged in theoretical investigations of wave propagation in dielectric waveguides.

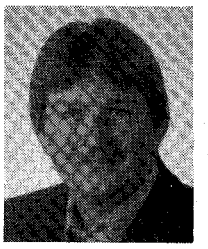

Norbert Schulz was born in Bremerhaven, Germany, on March 5, 1958. He received the Dipl. Ing. degree in electrical engineering from the University of Bremen, Germany, in 1983.

His research activities are in the field of dielectric waveguides. Since 1983, he has been with the Microwave Department of the University of Bremen.

Fritz Arndt (SM'83) was born in Konstanz, Germany, on April 30, 1938. He received the Dipl. Ing., the Dr. Ing., and the Habilitation degrees from the Technical University of Darmstadt, Germany, in 1963, 1968, and 1972, respectively.

From 1963 to 1973, he worked on directional couplers and microstrip techniques at the Technical University of Darmstadt. Since 1972, he has been a Professor and Head of the Microwave Department at the University of Bremen, Germany. His research activities are in the area of the solution of field problems of waveguide, finline, and optical waveguide structures, of antenna design, and of scattering structures.

Dr. Arndt is member of the VDE and NTG (Germany). He received the NTG award in 1970, and the A.F. Bulgin Award (together with three coauthors) in 1983 from the Institution of Radio and Electronic Engineers.